Three-dimensional analytical infinite order sudden quantum theory for triatomic photodissociation: Dependence on initial rotational and vibrational state and on thermal averages for NOCl dissociation on $T_1(1\,^3A')$ surface

Horacio Grinberg, Carl J. Williams, and Karl F. Freed

Citation: The Journal of Chemical Physics **100**, 9215 (1994); doi: 10.1063/1.467257
View online: https://doi.org/10.1063/1.467257
View Table of Contents: http://aip.scitation.org/toc/jcp/100/12
Published by the American Institute of Physics

Three-dimensional analytical infinite order sudden quantum theory for triatomic photodissociation: Dependence on initial rotational and vibrational state and on thermal averages for NOCl dissociation on $T_1(1\ ^3A'')$ surface

Horacio Grinberg,[a] Carl J. Williams, and Karl F. Freed
James Franck Institute and Department of Chemistry, The University of Chicago, Chicago, Illinois 60637

(Received 18 January 1994; accepted 1 March 1994)

Our previously developed analytical infinite order sudden quantum theory of triatomic photodissociation is generalized to compute fragment internal energy distributions when the initial triatomic rotational state has $K\neq 0$. The dependence of product rotational energy distributions on initial rotational and vibrational state is illustrated through model computations for the direct NOCl photodissociation from the ground to the $T_1(1\ ^3A'')$ potential energy surface. The calculations consider all $J,K\leqslant 9$ and employ a repulsive potential that is fit to *ab initio* computations. Comparisons of fragment rotational distributions with previous semiclassical approximations further elucidate the role of the mapping of the initial state bending wave function onto the fragment rotational distributions and the influence of parent rotations on this mapping. The infinite order sudden quantum-mechanical distributions exhibit a more complex structure, but upon thermal averaging they are already transformed at $T=3$ K into fairly broad rotational distributions. The present theory readily permits the calculations of energy distributions for initial states of high J and K.

I. INTRODUCTION

Theories for the photodissociation of triatomic molecules are progressing through a natural succession of stages. The first theories have been constructed based on simple models that attempt to elucidate generic properties of the photodissociation process and thereby to guide the interpretation and design of experiments.[1–4] The earliest such models use one-dimensional impulsive, Franck–Condon, etc., approximations,[5] while subsequent models confront the full multidimensionality of the triatomic photodissociation. The next stage in the maturation of our theoretical understanding is associated with the development of accurate computational schemes for numerically solving the Schrödinger equation governing the photodissociation dynamics, a stage that currently permits including three internuclear degrees of freedom in modeling the dissociation. When applied to triatomic molecules, the full numerical treatment is generally restricted to initial triatomic states of low total angular momentum quantum numbers $J\approx 0$.[6] Given the ability of numerically solving the three-dimensional Schrödinger equation, a final state of development involves the resurrection of simple models[7–17] to determine which successfully reproduce exact numerical solutions in specific limits,[18,19] so that these tested models are available for more routine usage in interpreting and predicting photodissociation experiments.

One important class of models centers around Franck–Condon, or sudden-type approximations. The first Franck–Condon model of Berry focuses on a single product vibrational mode and an "effective" vibration for the same coordinate in the initial bound state of the polyatomic molecule.[21] The more sophisticated Franck–Condon models of Freed *et al.*[14,22–25] account for the fact that the product and initial state vibrational modes, in general, differ and that the reaction coordinate cannot be described by a single normal mode in the initial bound molecular state. The difference between the natural coordinates for the initial bound and final dissociative potential surfaces thereby provides one mechanism for imparting vibrational excitation to the photofragments. An additional mechanism arises from the presence of final state interactions between the receding photofragments on the dissociative potential surface, interactions that can and often do alter the nascent energy distributions produced by the sudden Franck–Condon excitation process.

The multidimensional Franck–Condon models[18–20] predict that diatomic fragment rotational distributions have structures reflecting the nodal patterns in the initial bound state bending vibration wave functions, a prediction subsequently verified by Reisler *et al.* in the indirect photodissociation of NOCl,[26,27] found in full three-dimensional quantum photodissociation calculations,[19,20] and explained for $J=0$ by the simpler (one-dimensional) reflection principle model of Schinke and co-workers.[5,28–32] The latter is, in fact, an approximation to the one-dimensional bending Franck–Condon integral in the bend–stretch approximation discussed below. The multidimensional Franck–Condon models, however, predict the diatomic fragment rotational distributions from the photodissociation of bent triatomic molecules to have an additional oscillatory contribution that is not observed experimentally. Various suggestions for the lack of observing the extra oscillations are associated with experimental data containing averages over fragment fine structure states and over the narrow range of initial rotational states for molecules in a supersonic jet.[26,27]

[a]Permanent address: Departamento de Física, Facultad de Ciencias Exactas y Naturales, Universidad de Buenos Aires; MCIC Consejo Nacional de Investigaciones Científicas y Técnicas (CONICET), República Argentina.

 0021-9606/94/100(12)/9215/13/$6.00

In order to obtain analytical tractability, the bent triatomic photodissociation Franck–Condon model of Morse and Freed[14,15] invokes several approximations that are lifted in the more general three-dimensional infinite order sudden model by Grinberg *et al.*[18,19] The improved treatment of Grinberg *et al.* lifts the prior assumptions of isotropic final potential energy surfaces and of the separation between initial bound state bending and stretching motions (called the bend–stretch approximation). The bend–stretch approximation is commonly invoked in numerical three-dimensional photodissociation computations because the initial bound state wave function is represented in these computations by basis set expansions involving functions of the Jacobi scattering coordinates, which are more appropriate for describing dynamics on the final dissociative surface than the normal mode-like coordinates usually used by spectroscopists to describe the bound state vibrations of polyatomic molecules. Thus, the bend–stretch approximation restricts the basis set expansion to separate two-dimensional expansions for the stretching functions and a one-dimensional expansion for the bending function. Infinite order sudden computations by Grinberg *et al.*,[19,20] on the other hand, provide examples for which the bend–stretch approximation is inadequate, a result which emphasizes the merits of theoretical methods based on the use of separate coordinate systems for describing the bound and dissociative surface motions. Recent full numerical three-dimensional quantum computations likewise lift this approximation. As noted above, Schinke's useful reflection principle is based on an approximation to the one-dimensional bending Franck–Condon factor with the assumption of the bend–stretch separation.

As the initial state rotational quantum number J increases, so does the number of basis functions (or the equivalent) required for full three-dimensional quantum photodissociation computations. Thus, these calculations are currently extremely costly for the large J required to perform inital state thermal averages appropriate to many realistic experiments. Consequently, the prior infinite order sudden model of Grinberg *et al.* is still useful to elucidate the influence of parent rotation and vibration on fragment rotational energy distributions since the computational labor involved in applying the model only scales with J roughly as $J+1$ or one-half of the degeneracy. This low order scaling arises because of the fully analytic character of the infinite order sudden theory of Grinberg *et al.* The combination of infinite order sudden and Airy approximations are shown by Grinberg *et al.* to analytically permit performing two of the integrations in the nonseparable three-dimensional transition amplitudes, leaving only one remaining integration. The last integration is converted to a fully analytical expression upon introduction of a quadrature formula. Hence, the theory of Grinberg *et al.* produces purely analytical, albeit lengthy, expressions for the rotational and vibrational energy distributions of the photofragments.[18,19]

One of our interests here is to extend our infinite order sudden theory[33–35] to study the temperature or number of rotational states necessary to wash out the predicted secondary oscillations in the fixed initial J diatomic fragment rotational distributions. This study requires computations for a number of J and K, which is nontrivial for even full numerical three-dimensional theories. Since the previous work of Grinberg *et al.* limits explicit consideration to $K=0$, a necessary prelude to the desired computations requires the evaluation of the infinite order sudden transition amplitudes for both J and its projection K different from zero, a technically difficult analytical problem owing to the presence of Wigner rotation matrices (or the equivalent Jacobi polynomials) in the integrands. Thus, Sec. II briefly reviews the infinite order sudden theory and the current generalization to $J,K\neq 0$. Illustrative computations in Sec. III describe the variation of product rotational distributions with initial rotational and vibrational states and with the initial rotational temperature. Computations are performed for nine initial vibrational states and all $J,K\leqslant 9$. The $K=0$ limit of the quantum-mechanical IOS rotational distributions are compared with previous semiclassical models.[14] The computations, for concreteness, use potential functions fit to the repulsive portion of the *ab initio* NOCl T_1 state potential surface[36] and assume a direct ground to T_1 state dissociation. However, our computations are still purely illustrative because of the indirect character observed for the NOCl T_1 state photodissociation.[26] Work is in progress on developing a generalization of the infinite order sudden theory to describe these indirect photodissociations.

II. THEORY

The different photodissociation processes, such as direct photodissociation, predissociation, vibrational predissociation, etc., may be described through the Hamiltonian

$$H=H_0+V_I, \tag{2.1}$$

where V_I is the interaction Hamiltonian which couples the bound and continuum eigenstates of H_0. If the dissociation inducing the coupling V_I is sufficiently weak, the usual Golden Rule expression for the dissociation rate Γ_{if} from initial bound or quasibound state $|i\rangle$ to the final state $|f\rangle$ is valid[1] and is given by

$$\Gamma_{if}=\frac{2\pi}{\hbar}|\langle i|V_I|f\rangle|^2. \tag{2.2}$$

In addition, we adopt the Born–Oppenheimer and Condon approximations. Thus, the initial $|i\rangle$ and final $|f\rangle$ states are written below as products of nuclear and electronic wave functions. The electronic matrix elements of V_I are taken to be only weakly dependent on the nuclear coordinates in the regions where the overlap of the initial and final vibrational functions $|i\rangle$ and $|f\rangle$ is nonzero.

A. Initial state wave function

The initial bound state nuclear wave function for the bent triatomic molecule is represented in terms of a basis set

TABLE I. Spectroscopic data and relevant parameters used in the model photodissociation NOCl→NO($X\,^2\Pi_{3/2}$)+Cl($^2P_{3/2}$).

ω_1=1799.7 cm^{-1}	N=O stretch (99%)
ω_2=332.0 cm^{-1}	N–Cl stretch (71%), ClNO bend (29%)
ω_3=595.9 cm^{-1}	N–Cl stretch (32%), ClNO bend (68%)
ω_{NO}=1903.68 cm^{-1}	
K_1=14.087 mdyn/Å	(N=O stretch)
K_2=1.243 mdyn/Å	(N—Cl stretch)
K_3=1.15 mdyn Å/rad^2	(ONCl bend)
$\bar{r}_{NO}$(NOCl)=1.15 Å	
$\bar{r}_{NCl}$=1.975 Å	
$\bar{\delta}$=2.007 rad	
$\bar{r}_{NO}$(N=O)=1.1508 Å	
ρ=0.8270	
η=0.8840	
$\bar{R}$=2.302 Å	
$\bar{\theta}$=0.8906 rad	
A=2.9582 cm^{-1}	
B=0.1865 cm^{-1}	
C=0.1754 cm^{-1}	
B_v(NO)=1.7 cm^{-1}	
β_0=2.3080 rad	

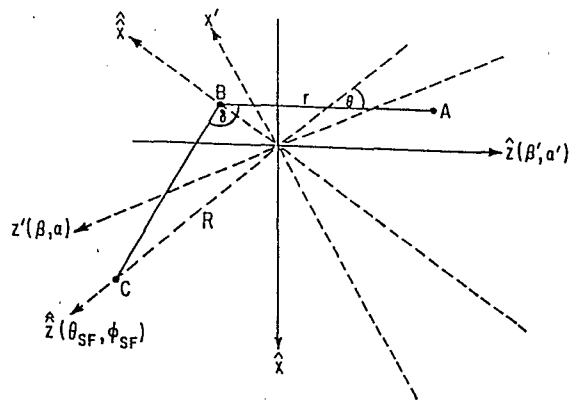

FIG. 1. Body-fixed coordinate systems for a bent triatomic molecule. The angles (β,α) give the orientation of the principal axis of smallest moment of inertia (along the z' axis), (θ_{SF},ϕ_{SF}) give the orientation of the atom to diatom vector (along the $\hat{z}$ axis), and (β',α') give the orientation of the diatomic molecule (along the $\hat{z}$ axis), all relative to the space-fixed frame. The $(\hat{x}\hat{y}\hat{z})$, $(x'y'z')$, and $(\hat{x}\hat{y}\hat{z})$ frames are all body-fixed frames specified with the z axis along the three vectors mentioned above. The molecular center of mass is located at the origin, and the diatomic center of mass is indicated by an asterisk. $R(\equiv Q_1')$ is the distance from atom C to the center of mass of the diatomic photofragment, and $r(\equiv Q_2')$ is the interatomic distance for A–B.

of rigid-rotor (asymmetric top),[37,38] harmonic oscillator functions

$$\Psi_i(Q)=\sum_K g_K[(2J+1)/8\pi^2]^{1/2} \times D^{J*}_{MK}(\alpha,\beta,\gamma)\prod_{i=1}^{3}\psi_{n_i}(Q_i), \tag{2.3}$$

where the wave functions for the asymmetric top are formed from linear combinations of the appropriate symmetric-top functions D^{J*}_{MK} with coefficients g_K.[39] The $\psi_{n_i}(Q_i)$ are harmonic oscillator wave functions in the normal coordinates Q_i,[40] and (α,β,γ) specify the Euler angles providing the orientation of the equilibrium principal axes of inertia relative to the space-fixed coordinate system.[37,38] Anharmonicities and vibration–rotation couplings may be included by taking linear combinations of harmonic basis functions of the form (2.3). Below we treat an individual harmonic term arising from the use of anharmonic potentials since the general case follows directly. Table I summarizes some of the spectroscopic data for the ground electronic state of NOCl. Notice that although the force constants for the initial vibrational potential energy do not contain cross terms between local mode bend and stretch, the ν_2 and ν_3 modes are mixtures of bend and asymmetric stretches due to the kinetic energy operator (G matrix)[41] coupling between bend and stretch. These bend–stretch couplings often qualitatively affect[20] predictions of fragment rotational energy distributions.

B. Final state wave function

Scattering coordinates are the most appropriate to describe the dynamics in the final repulsive electronic state. Thus, the asymptotic limit $Q_1'\to\infty$ of the nuclear wave function on the final electronic surface is written in the scattering coordinate basis as

$$\Psi_f(Q')\to\psi_{n_4}(Q_2')\psi_{\hat{E}}(Q_1';\theta) \times\sum_{\mu,m}\langle J'M'|lj\mu m\rangle Y_{jm}(\beta',\alpha')Y_{l\mu}(\theta_{SF},\phi_{SF}), \tag{2.4}$$

where $\psi_{n_4}(Q_2')$ is a harmonic oscillator function for the separated diatomic photofragment. The angular momenta (j,m) and (l,μ) refer to the rotation of the diatomic fragment and its z component and the orbital motion of the atom relative to the diatomic center of mass and its z component, respectively. The angles (β',α') are the polar and azimuthal angles specifying the orientation of the diatomic molecule relative to space-fixed axes, while (θ_{SF},ϕ_{SF}) give the orientation of the atom–diatom vector relative to the space-fixed frame (see Fig. 1). Assuming that no electronic angular momentum is present these two angular momenta l and j are coupled to give well-defined values of the total angular momentum and its z component (J',M') using the Clebsch–Gordan coefficients $\langle J'M'|lj\mu m\rangle$.[37,38,42] Finally $\psi_{\hat{E}}(Q_1';\theta)$ is the asymptotic continuum wave function for the relative translational motion of the photofragments with asymptotic kinetic energy $\hat{E}$. Below this fragment wave function $\psi_{\hat{E}}(Q_1';\theta)$ is taken to be given by infinite order sudden (IOS) and Airy approximations, as described previously.[19] Here Q_1' and θ are, respectively, the distance between the diatom center of mass and the atom and the angle between the diatomic axis and the atom to diatom vector (Fig. 1).

The infinite order sudden approximation applies when the dissociation proceeds rapidly compared to diatomic rota-

tional times. Hence, the atomic fragment essentially moves in a straight line trajectory with the diatomic at fixed orientation. An average is then performed over all relative orietations of the diatomic with respect to the direction of the atom's motion. An equivalent representation of the IOS approximation considers the asymptotic fragment kinetic energy to be far in excess of the diatomic rotational energies, so that the diatomic rotational energy may be neglected with respect to the kinetic energy. This IOS approximation then results in the approximate wave function taking on the the asymptotic form of Eq. (2.4). Corrections to this approximation become important at low asymptotic kinetic energies and when there are substantial torques exerted in the exit channel.

C. Potential energy surface

The initial bound state is taken as the ground electronic state with spectroscopic constants summarized in Table I. The dissociative potential energy surface is fit to *ab initio* calculations for the repulsive portion of the $T_1(1\ ^3A'')$ state potential for NOCl as provided in Ref. 36. The fit is obtained using the functional form

$$U(R;\theta)=F(\theta)\exp[-(R-\bar{R})f(\theta)], \tag{2.5}$$

where $f(\theta)$ and $F(\theta)$ are numerically determined with a cubic spline fit. In Eq. (2.5), R is the distance of atom C (the Cl atom) to the center of mass of the diatom A–B (the NO diatomic photofragment), and $\bar{R}$ is the corresponding equilibrium distance.

D. Evaluation of multidimensional transition amplitudes

Our previous paper[19] presents the relations between normal and scattering coordinates as well as the details for the analytical evaluation of the integrals involving the coordinates r (interatomic distance of the diatomic photofragment) and R. The rotational distributions are evaluated using the Condon approximation and ignoring the dependence of the scattering wave function $\psi^*_{\bar{E}}(R;\theta)$ on orbital angular momentum l. In order to alleviate the computational complexity inherent in the calculation of the matrix element in Eq. (2.2), two other approximations are required for analytical tractability: (a) the infinite order sudden (IOS) approximation is used for the rotational motions, and (b) an Airy function approximation is introduced for the rotational IOS wave functions. We assume dipole coupling (direct photodissociation) and approximate the rotational motions by symmetric top functions (see discussion below). This then permits elimination of the sum over K in Eq. (2.3). Following the steps leading to Eq. (3.8b) of Ref. 14, the rotational angular momentum distributions $P_{JK}(j)$ are obtained for the present case as

$$P_{JK}(j)=V_I^2(j+1/2)\sum_{m\lambda}\left|\int_{-\infty}^{\infty}dr\int_0^{\infty}dR\int_0^{\pi}d\theta\right.$$
$$\times\psi^*_{n_4}(r)\psi^*_E(R;\theta)d^1_{\lambda 0}(\Omega)d^j_{0m}(\theta)d^J_{m-\lambda K}(\phi_2+\beta_0$$
$$\left.-\bar{\theta})|J_B|^{1/2}\prod_{i=1}^{3}\psi_{n_1}(Q_i)\right|^2, \tag{2.6}$$

where the transformation $Q_i=Q_i(r,R,\theta)$ is discussed below. The quantum numbers J and K specify the initial (bound) rotational state; j is the diatomic fragment rotational quantum number; and λ designates the polarization of the incident light with respect to space-fixed coordinates. d^j_{0m} and $d^J_{m-\lambda K}$ are Wigner rotation matrix elements which can be expressed in terms of normalized associated Legendre polynomials,[37,38]

$$d^j_{0m}(\theta)=(j+1/2)^{-1/2}P^m_j(\cos\theta), \tag{2.7}$$

and Jacobi polynomials,[37] respectively (see below). J_B is the Jacobian of transformation from initial bound state normal coordinates Q_i ($i=1, 2, 3$) to the Jacobi scattering coordinates (r,R,θ) on the repulsive potential energy surface. Details of this transformation and the different coordinate systems along with the relation between them are given in previous papers.[14,19] Here it is enough to note that if θ is the angle between the diatomic axis and the atom to diatomic molecule center of mass vector (see Fig. 1), it can be shown that[14]

$$\theta=\phi_1-\phi_2+\bar{\theta}, \tag{2.8}$$

where $\bar{\theta}$ is the equilibrium angle in the initial bound state configuration, and ϕ_1 and ϕ_2 describe, respectively, the angular displacements of the diatomic vector and of the atom to diatom vector of the vibrating molecule from their equilibrium bound state positions as defined by the appropriate Eckart frames.[14] The angles (ϕ_1,ϕ_2) are functions of the internal coordinates of the molecule, and both ϕ_1 and ϕ_2 vanish, by definition, for the bound state equilibrium geometry. In principle, ϕ_1 and ϕ_2 and θ depend on all three coordinates (r,R,δ), but as long as stretching vibrations have displacements that are much smaller than bending amplitudes, the dependences on R and r can be ignored. Thus, we adopt the leading linear approximations[14]

$$\phi_1=\rho(\delta-\bar{\delta}), \tag{2.9}$$

$$\phi_2=\left[\rho-\left(\frac{\partial\theta}{\partial\delta}\right)_{\rm eq}\right](\delta-\bar{\delta}), \tag{2.10}$$

where $(\delta-\bar{\delta})$ is the instantaneous displacement of the bond angle relative to the equilibrium angle in the initial bound state configuration of the molecule. The molecular parameter ρ can be determined from the Eckart and center of mass conditions as a function of the atomic masses and interatomic distances of the initial bound molecular state.[14] After some rather involved algebra, ρ is obtained as

$$\rho=\frac{m_C\bar{r}_{BC}[(m_A+m_B)\bar{r}_{BC}-m_A\bar{r}_{AB}\cos\bar{\delta}]}{m_C(m_A+m_B)\bar{r}^2_{BC}-2m_Am_C\bar{r}_{AB}\bar{r}_{BC}\cos\bar{\delta}+m_A(m_B+m_C)\bar{r}^2_{AB}}, \tag{2.11}$$

where $\bar{r}_{AB}$ and $\bar{r}_{BC}$ are the equilibrium bonds length of the AB and BC bonds in the initial bound molecular state $|i\rangle$, and m_i is the mass of atom i. The angle β_0 in Eq. (2.6) is evaluated from the diagonalization of the inertia tensor for the initial bound state of the triatomic molecule and is found to be given by

$$\beta_0=(1/2)\arctan[-2I_{xy}/(I_{xx}-I_{yy})], \tag{2.12}$$

where the bond of the diatomic fragment A–B is along the x axis, I_{xy} is the product of inertia, and I_{xx} and I_{yy} are the moments of inertia about the x and y axes, respectively. For transitions polarized in the plane of the molecule, Ω in Eq. (2.6) is given by[15]

$$\Omega=\beta_0+\beta''+\phi_1-\theta, \tag{2.13}$$

where β'' is the Euler angle which rotates the body-fixed frame (x',y',z'), whose axes are coincident with the principal axes of inertia, into the body-fixed frame (x'',y'',z''), with z'' along the transition dipole for the photodissociative transition. The (x'',y'',z'') axis system can be visualized with reference to Fig. 1, where this axis is not explicitly represented to avoid clutter in the figure. This axis system is simply obtained by rotating the $\hat{z}$ axis in the plane of Fig. 1 to now point along the direction of the in-plane transition dipole (not shown in Fig. 1).

This paper studies fragment rotational distributions as functions of initial triatomic rotational and vibrational states and temperatures. Thus, it is necessary to evaluate Eq. (2.6) for $K\neq 0$, and this requires expressing the asymmetric top wave functions in terms of symmetric top functions with the unique axis in the plane of the molecule. The rotational constants for NOCl in Table I indicate that this molecule is a near prolate symmetric top (A>B~C). The solution of the Schrödinger equation for such a system can be expressed in terms of Jacobi polynomials,

$$d^J_{mK}(\theta)=M_{JKm}x^{|K-m|/2}(1-x)^{|K+m|/2}\times P^{|m-K|,|m+K|}_{J-|K+m|/2-|K-m|/2}(z), \tag{2.14}$$

where the normalization factor M_{JKm} is given by

$$M_{JKm}=\left[\frac{(J+|K+m|/2+|K-m|/2)!(J-|K+m|/2-|K-m|/2)!}{(J-|K+m|/2+|K-m|/2)!(J+|K+m|/2-|K-m|/2)!}\right]^{1/2} \tag{2.15}$$

and

$$x=(1-z)/2, \quad z=\cos\theta.$$

The numerical evaluation of the Jacobi polynomials $P_n^{p,q}(x)$ involves using the relation[43]

$$P_n^{p,q}(x)=\binom{n+p}{n}a_0(x), \tag{2.16}$$

with $a_0(x)$ determined recursively from

$$a_{m-1}(x)=1-(b_m/c_m)f(x)a_m(x)$$

$$[m=n,n-1,\ldots,2,1;a_n(x)=1], \tag{2.17}$$

where

$$b_m=(n-m+1)(p+q+n+m);$$

$$c_m=2m(p+m); \quad f(x)=1-x. \tag{2.18}$$

The above choices for the wave functions in the initial and final states produce three-dimensional nonseparable transition amplitudes which are reduced to analytical forms by introduction of the IOS and Airy function approximations for rotational motions and the continuum wave functions. In fact, as long as vibrational motions are described by harmonic oscillator wave functions, the analytical integration over the scattering coordinate r (interatomic distance of the diatomic photofragment) can be straightforwardly performed. The result is a Gaussian function of R and θ. In order to treat the integral over R analytically, the potential energy surface of Eq. (2.5) is first linearized around the classical turning point.[19] The Schrödinger equation with this linear potential admits a solution in terms of the Airy function, thus allowing the integral over the radial coordinate R to be performed analytically, after use of the integral representation for the Airy function.[8] This leaves only the integral over θ, which is converted to analytical form by introducing a Gaussian–Legendre quadrature procedure. While the details are rather involved,[19] the final results are algebraic expressions that are readily evaluated numerically.

III. RESULTS AND DISCUSSION

The present calculations consider the model direct photodissociation from NOCl in the $T_1(1\ ^3A'')$ state to produce NO($X\ ^2\Pi_{3/2}$). The geometry, valence force constants, and normal mode frequencies for the initially ground NOCl state and for the $X\ ^2\Pi_{3/2}$ electronic state of NO are taken from Refs. 44 and 45 and are provided in Table I along with other relevant parameters. The present IOS model ignores inelastic scattering processes on the repulsive surface. Thus, the model in Eq. (2.4) effectively assumes that the dissociation direction is along the atom to diatomic molecule vector. Since NOCl belongs to the C_s symmetry group, only two types of transitions exist with symmetries A' (where the transition dipole moment μ lies in the molecular plane) and A'' (where μ is perpendicular to the molecular plane).

The direction of the transition dipole moment in the molecule must be properly defined. The index λ in Eq. (2.6) is zero for linearly polarized light and yields parallel transitions, while circularly polarized light and perpendicular transitions emerge from $\lambda=\pm 1$. Thus, there is one type of photofragment rotational distribution produced when the transition dipole is along the atom to diatom vector (with $\Omega=0$) and another when the transition dipole is perpendicu-

lar to this vector (with $\Omega=\pi/2$). For the NOCl case, we assume the transition dipole lies along the NO bond, so that $\beta_0=-\beta''$. Equation (2.13) then yields $\Omega=\phi_1-\theta$ and therefore the resulting rotational distributions are linear combinations of those from parallel and perpendicular transitions.

Normalized, thermally averaged rotational distributions are calculated from

$$P_j(T)=\frac{I(j;T)}{\Sigma_j I(j;T)}, \tag{3.1}$$

where $I(j;T)$ is given by

$$I(j;T)=\sum_{J=0}^{N_{\max}}\sum_{K=0}^{J}(2J+1)P_{JK}(j)\exp(-E_{JK}/kT), \tag{3.2}$$

with the unnormalized rotational distributions $P_{JK}(j)$ determined from Eq. (2.6). T is the absolute temperature, and the initial state rotational energy is

$$E_{JK}=(1/2)(B+C)J(J+1)+[A-(1/2)(B+C)]K^2 =E_{J,-K}. \tag{3.3}$$

The present calculations include states of total angular momentum J from $J=0$ through $J=9$ in Eq. (3.2). The IOS approximation applies when the total energy E is much larger than the rotational energy $B_v j(j+1)$ for all states populated during the fragmentation process, a condition well satisfied in the present calculations for lower j, but some errors may arise in the higher j tails of the $P_{JK}(j)$ distribution where almost all the available energy goes into fragment rotation.

In order to emphasize the influence of parent internal excitations on product state distributions, computations have been performed for excitation originating from nine excited vibrational states of the ground electronic state and for several temperatures. Thermal averages are evaluated for each vibrational state separately since vibrations are generally not totally thermalized in a supersonic jet. The upper surface available energy is presented in Table II for each initial vibrational state.

TABLE II. Available fragment and photon energies for initial vibrational states in the model photodissociation NOCl→NO($X\,^2\Pi_{3/2}$)+Cl($^2P_{3/2}$).

Vibrational state	E_{av}[a] (eV)	Photon energy[b] (cm^{-1})
(0,0,0,0)	0.3823	16 206
(0,0,1,0)	0.4324	16 611
(0,0,2,0)	0.4849	17 035
(1,0,0,1)	0.3385	17 730
(1,0,1,1)	0.3864	18 115
(1,0,2,1)	0.4364	18 519
(2,0,0,2)	0.3053	19 306
(2,0,1,2)	0.3470	19 646
(2,0,2,2)	0.3900	20 000

[a]Calculated from $E_{av}=h\nu-D_0-E_v(\mathrm{NO})-E_{el}(\mathrm{NO})$ where $h\nu$ is the photon energy, D_0 is the dissociation threshold (13 000 cm^{-1}) (see Ref. 46), $E_v(\mathrm{NO})$ is the energy of the NO vibration, and $E_{el}(\mathrm{NO})$ is the NO spin–orbit electronic energy (123 cm^{-1}) [see Ref. 26(b)].
[b]Taken from Ref. 26(b).

The WKB approximation of Morse and Freed[14] yields a simplified, physically transparent analytical expression for $P_{JK=0}(j)$. When (a) the initially bound state of the triatomic molecule is a symmetric top, (b) the bend–stretch approximation is invoked, (c) the dissociative potential surface is isotropic, and (d) when $K=0$, this WKB approximation displays both the mapping of the ground state bending contribution $P_{J0}(j)$ along with the additional higher frequency oscillations whose washing out upon averaging we wish to study. Thus, comparisons between the quantum-mechanical rotational distributions computed from Eq. (2.6) and this semiclassical approximation help to illustrate the role of this bending wave function mapping. Taking the particular case of parallel transitions the Morse–Freed WKB approximation for $P_{J0}(j)$ is given by

$$P_{J0}(j)\propto\left(\frac{2j_<+1}{2J+1}\right)\left\{\sin^2\left[(J+j+1)\bar{\theta}-(J+1/2)\beta_0+\frac{\pi}{4}+(-1)^{n_3}\frac{\pi}{4}\right]\left[H_{n_3}\left(\frac{(J+j+1)\eta-(J+1/2)\rho}{M_{33}}\right)\right]^2\right.$$
$$\times\exp\left[-\left(\frac{(J+j+1)\eta-(J+1/2)\rho}{M_{33}}\right)^2\right]+\sin^2\left[(J+1/2)\beta_0+(j-J)\bar{\theta}-\frac{\pi}{4}+(-1)^{n_3}\frac{\pi}{4}\right]$$
$$\left.\times\left[H_{n_3}\left(\frac{(J+1/2)\rho+(j-J)\eta}{M_{33}}\right)\right]^2\exp\left[-\left(\frac{(J+1/2)\rho+(j-J)\eta}{M_{33}}\right)^2\right]\right\}, \tag{3.4}$$

where $j_<$ is the minimum of J and j and where η is given in the δ representation[19] by

$$\eta=\left(\frac{\partial\theta}{\partial\delta}\right)_{eq}=\frac{\bar{r}_{BC}}{\bar{r}_{BC}-\gamma\bar{r}\cos\bar{\delta}}; \tag{3.5}$$

with $\gamma=1/(1+m_B/m_A)$, and with M_{33} obtained from Eq. (2.7) of Ref. 19 as

$$M_{33}=(\omega_3/\hbar)^{1/2}/\eta, \tag{3.6}$$

where ω_3 is the frequency of the bending mode (see Table I). Both terms in Eq. (3.4) contain similar factors which are the squares of a Hermite polynomial times a Gaussian function and which are merely the square of the momentum representation of the ground state bending wave function. The additional sinusoidal oscillatory factors in Eq. (3.4) are associ-

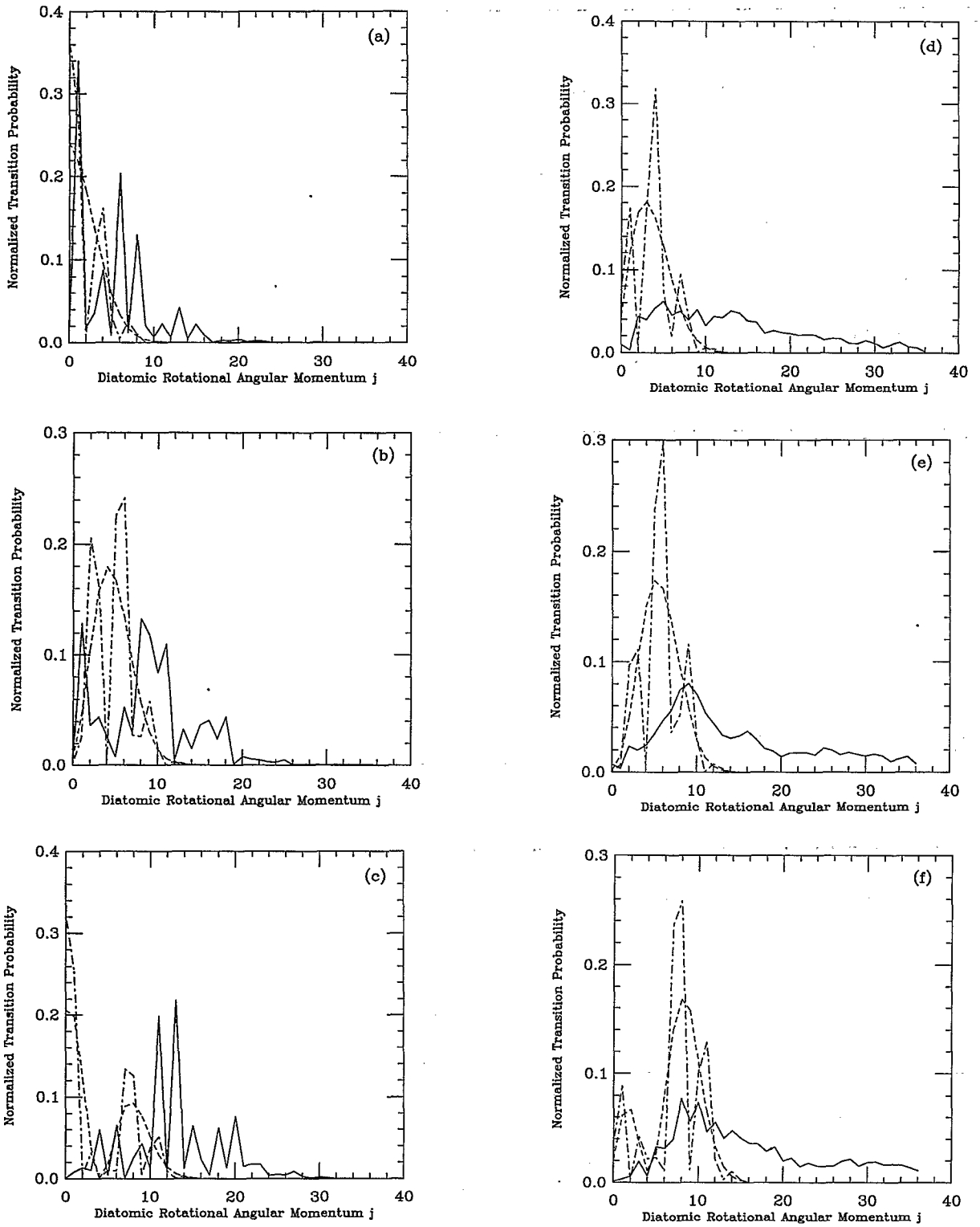

FIG. 2. Normalized rotational distributions for the model photodissociation NOCl→NO($X\ ^2\Pi_{3/2}$)+Cl($^2P_{3/2}$) under dipole coupling. (—) quantum-mechanical IOS calculations; (·····) semiclassical WKB approximation; (---) mapping of bending wave function. (a) $J=0$, $K=0$; $n_1=n_2=n_4=0$, $n_3=0$. (b) Same as (a), but $n_3=1$. (c) Same as (a), but $n_3=2$. (d) $J=9$, $K=0$; $n_1=n_2=n_4=0$, $n_3=0$. (e) Same as (d), but $n_3=1$. (f) Same as (d), but $n_3=2$.

ated with the probability that the dissociation of a molecule along the direction described by $\bar{\theta}$ finds an orbital angular momentum state l. Schinke's reflection principle has been used to obtain an approximation to Eq. (3.4) for $J=0$ only.

Figure 2 displays three different computations of the normalized $P_{J0}(j)$ for excitation from the vibrational states $(0,0,n_3)$ (a progression in the bending vibration n_3) with the initial total angular momentum $J=0$ and $J=9$ and with n_4, the final diatomic vibrational quantum number, taken to be 0. The solid line presents our full quantum computations from

Eq. (2.6); the dot–dashed lines are obtained from the semiclassical WKB approximation of Eq. (3.4); and finally the dashed lines come from Eq. (3.4) with the $\sin^2$ factors omitted. Thus, the dashed lines provide the mapping of the ground state bending wave function onto $P_{J0}(j)$ for comparison with the other two descriptions. For instance, consider first $J=K=0$. The dashed line in Fig. 2(a) displays the Fourier transform of the $n_3=0$ ground bending function, while the WKB approximation (dot–dash) curve imposes the higher frequency oscillations but retains the overall width and shape of the rotational distributions. The intensity of the highest peak in the semiclassical approximation is almost the same as that predicted by the full quantum calculations. The semiclassical approximation also succeeds well in predicting the locations of the first node and second peak at $j=4$. However, the infinite order sudden (solid curve) quantum-mechanical calculation has more complicated structure and is broadened somewhat from the WKB approximation. These changes emerge in the infinite order sudden (IOS) quantum calculations from the presence of coupling [neglected in deriving Eq. (3.4)] between bends and stretches in the initial bound state, couplings which have been shown by us in a previous work[19,20] as possibly substantially altering $P_{JK}(j)$. Other contributing factors to the difference between the IOS quantum and WKB approximations include the anisotropy of the repulsive potential surface, and the incorporation of slowly varying factors, such as the $d^1_{\lambda 0}(\Omega)$ in Eq. (2.6) and the θ-dependent part of the Jacobian in Eq. (2.6),

$$|J_B|^{1/2}=\left|\frac{\bar{R}(\bar{R}-\gamma\bar{r}\cos\theta)/\sin\theta}{\bar{R}^2+\gamma^2\bar{r}^2-2\bar{R}\gamma\bar{r}\cos\theta}\right|^{1/2}. \tag{3.7}$$

Figure 2(b) presents normalized rotational distributions produced by excitation from the the first excited bending state $n_3=1$ of the ground electronic state. The example in Fig. 2(b) shows similar trends to those found for $n_3=0$ in Fig. 2(a). The dashed line in Fig. 2(b) exhibits the influence of the node in the ground electronic state $n_3=1$ bending wave function at $\delta=\bar{\delta}$, which translates to the node in $P_{00}(j)$ at $j=0$, while the WKB approximation superimposes the oscillations of Eq. (3.4). The IOS computations (solid line) are again more structured and somewhat broader than the WKB approximation. The general rotational distribution shifts to higher j with increasing excitation of the ground state bend. This shift is a result of the mapping of the bending wave functions as in Eq. (3.4) but again with some additional broadening. Similar patterns appear in Fig. 2(c) for $n_3=2$ (zero vibrational angular momentum) and $J=0$, but there is even more pronounced broadening of $P_{J0}(j)$ with respect to the semiclassical approximations, probably due to errors associated with the bend–stretch approximation used in deriving Eq. (3.4). Excitation of initial state rotational motion to $J=9$ in Figs. 2(d), 2(e), and 2(f) shifts the $n_3=0$ dashed peak to $j=4$, consistent with the simple semiclassical arguments of Ref. 14 that the initial state angular momentum is partitioned (unequally) between fragment rotation and orbital angular momenta. Apart from this shift in the peak, the transition between the three curves in Fig. 2(d) displays similar trends as for $J=0$. The underlying initial state bending wave function, however, is no longer readily discernible in the full calculations (solid lines) for $J=9$. The semiclassical rotational distributions, on the other hand, roughly reflect the nodal patterns of the initial state bending wave function. The small shift in $P_{J0}(j)$ with J indicates that the main source of fragment NO angular momentum is still from the mapping of the NOCl ground state bending wave function. However, now the motions along θ are no longer separate from pure stretches, so the "effective" bending along θ is more complicated and leads to the departures from the simple WKB approximation.

Figure 3 presents the normalized rotational distributions obtained for excitation from the bending progression $n_3=0$, 1, 2 for $K=4$ and 7 and for various total angular momenta J. No apparent ground state bending wave function structure is discernible in these figures, apart from the general shifting to higher j of the rotational distributions with increasing excitation in the ground state bend. This shifting to higher j with larger n_3 arises because the wider angular spread of the higher bending functions which upon Fourier transform translates to a wider j range in $P_{JK}(j)$. Oscillatory structure is still present in Fig. 3 but tends to become washed out at higher K, especially for $J=K$, probably due to initial state bend–stretch couplings and the anisotropy of the potential which makes the scattering wave function $\Psi^+_E(Q'_1;\theta)$ of Eqs. (2.4) and (2.6) dependent on the bending angle. This is particularly evident for higher total angular momentum states, as is clearly seen, e.g., when $K=J=7$ in Figs. 3(d)–3(f).

Computations have been performed for cases in which there is initial excitation in the symmetric NO stretch in NOCl (with $n_1=0$, 1, 2 but with the NO fragment unexcited $n_4=0$) and also for others in which the fragment NO stretch is excited with $n_4=0$, 1, 2 (but with no fragment excitation $n_1=0$). All these cases also consider initial excitation of the bending vibration with $n_3=0$, 1, or 2, and J and K range separately from 0 to 9. The normalized rotational distributions in all these cases are almost identical to those obtained for the same n_3, J, and K but for $n_1=n_4=0$. However, Fig. 4 illustrates the differences from the $n_1=n_4=0$ case which begin to emerge for $n_1=n_4=1$ or 2, corresponding to initial state excitation in the symmetric NO stretch and the fragments produced with the same NO excitation. The differences between the $n_1=n_4=1$ or 2 examples and those for $n_1=n_4=0$ are very slight when $n_3=0$, but become evident when $n_3\neq 0$. Particularly interesting is the structure of the rotational distributions for $J=K$. When $J=K=4$ [Figs. 4(a)–4(c)], excitation of the bending mode to $n_3=1$ or 2 produces a shifting of the highest peak to larger j, but there is very similar structure to the rotational distributions produced from both initial stretching vibrational states. Basically, the relative intensities are changed, but not the structure of the normalized $P_{JK}(j)$. For higher $J=K$, e.g., $J=K=9$ [Figs. 4(d)–4(f)], the structured pattern is completely washed out, as previously noted for $n_1=n_4=0$ and $J=K=7$ in Fig. 3(d). The two different rotational distributions in each of Figs. 4(d)–4(f) are very similar but again are shifted to larger j for excitation from the excited bending states $n_3=1$ and 2. However, while the peak in the rotational distribution function for $n_1=n_4=1$ moves to higher j for

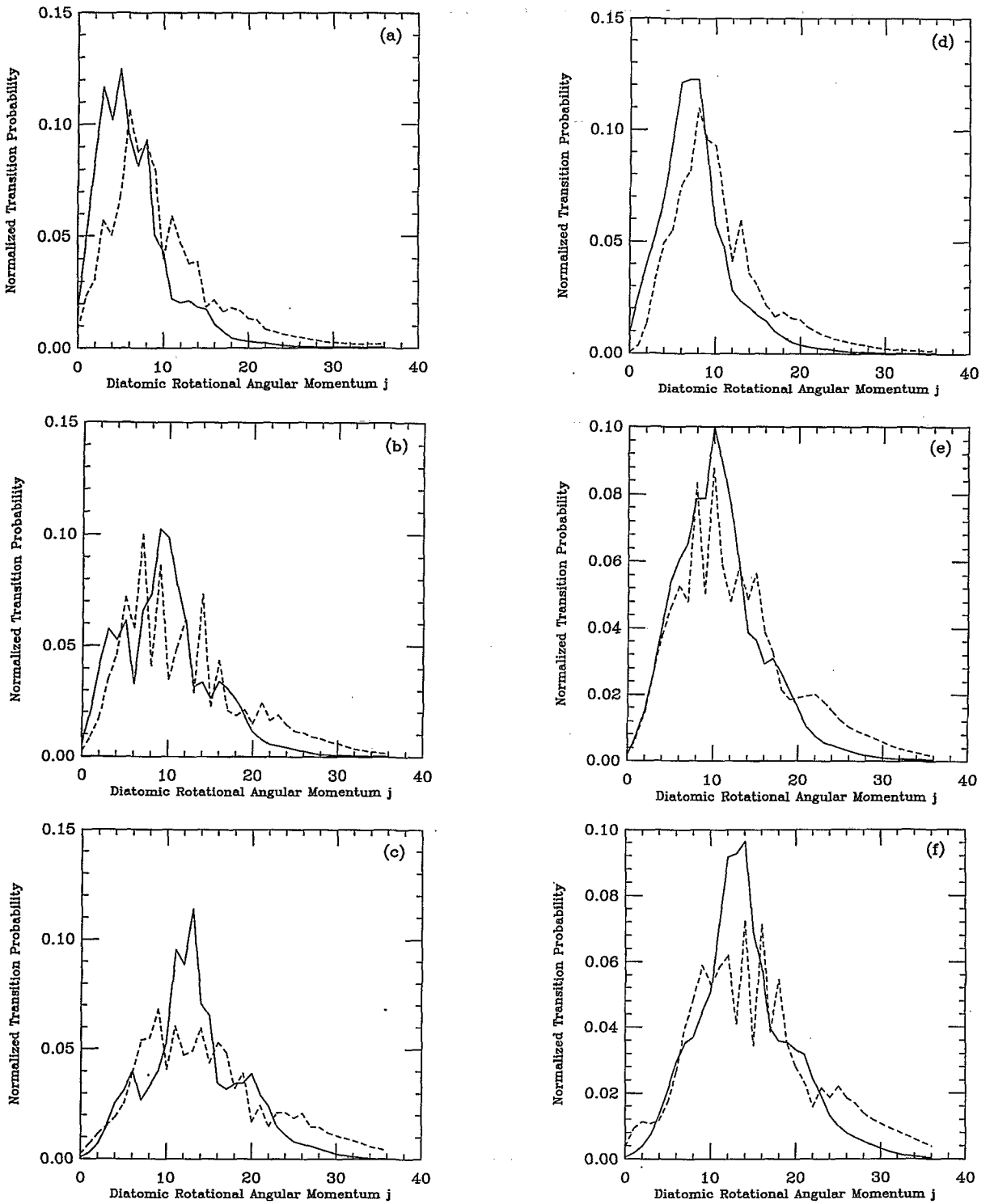

FIG. 3. Normalized IOS quantum-mechanical rotational distributions for the model photodissociation $NOCl \rightarrow NO(X\ ^2\Pi_{3/2}) + Cl(^2P_{3/2})$ under dipole coupling. (a) (—) $J=4$, $K=4$; (---) $J=7$, $K=4$; $n_1=n_2=n_4=0$, $n_3=0$. (b) Same as (a), but $n_3=1$. (c) Same as (a), but $n_3=2$. (d) (—) $J=7$, $K=7$; (---) $J=9$, $K=7$; $n_1=n_2=n_4=0$; $n_3=0$. (e) Same as (d), but $n_3=1$. (f) Same as (d), but $n_3=2$.

$n_3=2$, it shifts to lower j for $n_3=1$, but the previous trend is found for the $n_1=n_4=2$ case. When $J=9$ and $K=7$ [Figs. 4(g)–4(i)], there is no variation in the position and intensity of the highest peak in the $n_1=n_4=1$ state rotational distribution for excitation from both the ground and first excited bending states. However, the intensity of the highest peak for $n_1=n_4=0$ is reduced and shifted to higher j in passing from $n_3=0$ to $n_3=2$. The $n_3=1$ example in Fig. 4(h) clearly displays identical structures to both $P_{JK}(j)$ but with altered intensities when the NO stretches are excited and unexcited. The computed differences between the $n_1=n_4\neq 0$ and $n_1=n_4=0$ cases must again arise primarily from the pres-

ence of bend–stretch couplings in the ground electronic state vibrational wave function.

The IOS model describes the rotational distribution produced by the sudden Franck–Condon absorption between electronic states with very different natural coordinate systems. However, as the molecule dissociates this initial IOS rotational distribution is changed by the interfragment torques $\partial U(R;\theta)/\partial\theta$ on the excited state potential $U(R;\theta)$ of Eq. (2.5). These final state interactions with even modest $\Delta j=\pm 1$ transitions could wash out the IOS calculated oscil-

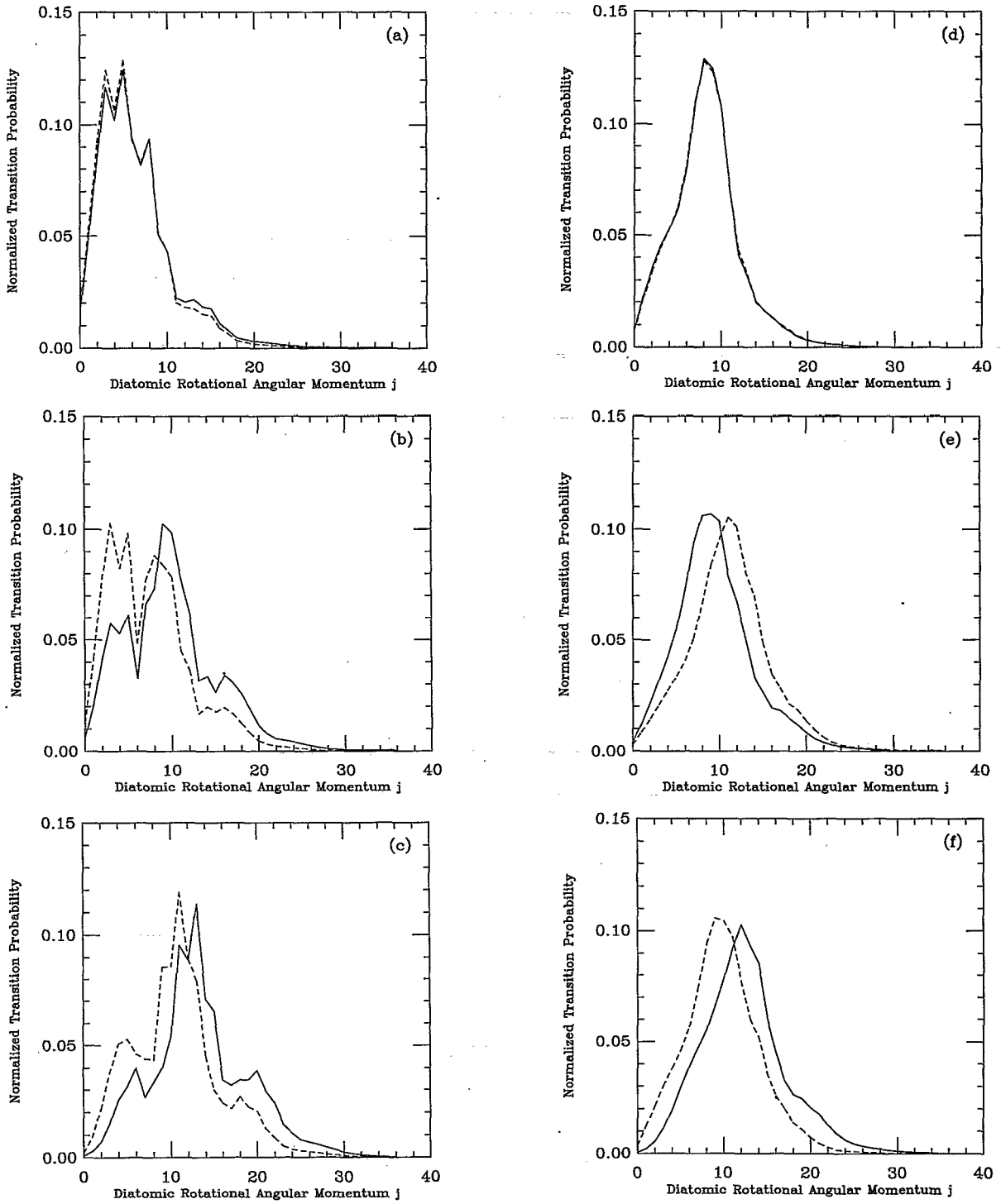

FIG. 4. Normalized IOS quantum-mechanical rotational distributions for the model photodissociation NOCl→NO($X\,^2\Pi_{3/2}$)+Cl($^2P_{3/2}$) under dipole coupling. (a) $J=4$, $K=4$; $n_2=0$, $n_3=0$; (—) $n_1=n_4=0$; (---) $n_1=n_4=1$. (b) Same as (a), but $n_3=1$. (c) Same as (a), but $n_3=2$. (d) $J=9$, $K=9$; $n_2=0$, $n_3=0$; (—) $n_1=n_4=1$; (---) $n_1=n_4=2$. (e) Same as (d), but $n_3=1$. (f) Same as (d), but $n_3=2$. (g) $J=9$, $K=7$; $n_2=0$, $n_3=0$; (—) $n_1=n_4=0$; (---) $n_1=n_4=1$. (h) Same as (g), but $n_3=1$. (i) Same as (g), but $n_3=2$.

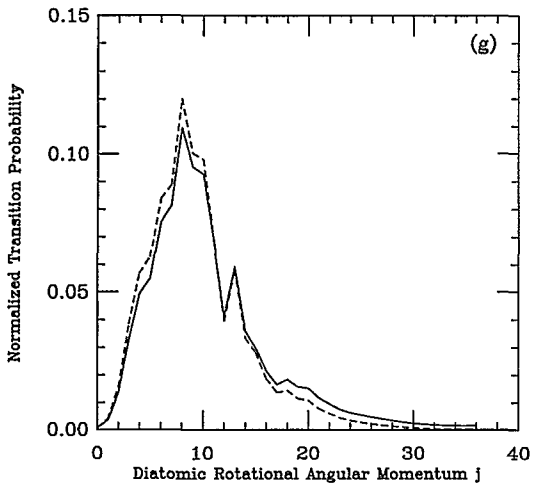

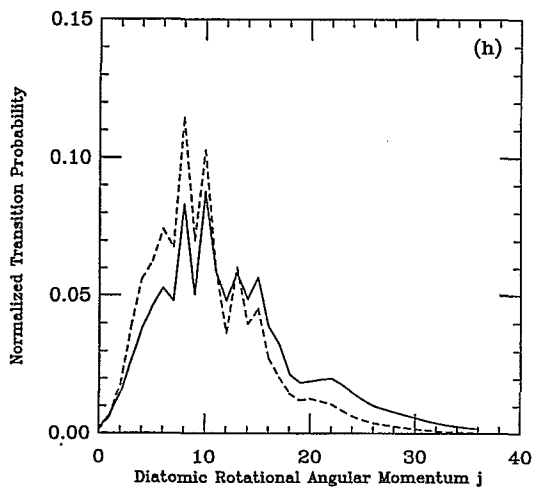

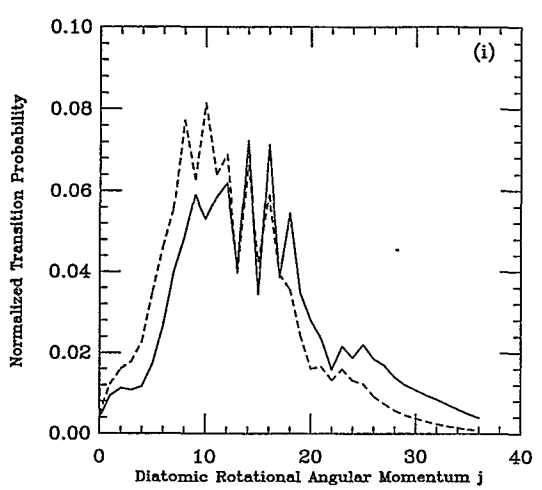

FIG. 4. (*Continued.*)

lations in $P_{JK}(j)$, since the computed oscillations are of high frequency. Nevertheless, we now continue to ignore the final state interactions and assess the influence of thermal averaging on the washing out of these oscillations and on the relationship of the thermally averaged rotational distributions to the mapping of the ground state bending wave functions.

Figure 5 displays the thermally averaged NO rotational distributions for given initial vibrational states and for excitation originating from the bending progression $n_3=0$, 1, 2 with $n_1=n_2=n_4=0$. There is still some structure in the individual thermal rotational distributions for $T=1$ or 2 K, but already for $T=3$ K the thermally averaged $P_j(T)$ become structureless single peak distributions. Comparing Fig. 5 with Fig. 2, it is clear that the widths of the thermally averaged distributions are considerably larger than those arising from the simply mapping of the bending wave function. As the initial state bend is progressively excited, the $T=3$ K rotational distributions peaks at higher j, consistent with the behavior of individual contributing J and K. A consideration of the processes with $n_1=n_4=1$ or $n_1=n_4=2$ yields trends in the thermal rotational distributions which again parallel those for the individual contributing J and K.

IV. CONCLUSIONS

This paper studies the model NOCl direct photodissociaiton process to the $T_1(1\ ^3A'')$ state using an extension of our previously developed three-dimensional analytical infinite order sudden (IOS) quantum-mechanical theory to include contributions for initial states with $K\neq 0$. Our computations use a realistic ground state basis set of rigid-rotor and harmonic vibrational wave functions of the natural normal modes, while the continuum state is taken as a product function in the natural Jacobi scattering coordinates appropriate to the dissociative surface. Although the ground state vibrational potential energy does not contain couplings between pure local mode bends and stretches, couplings present in the kinetic energy operator[41] imply that the ground state normal modes cannot generally be represented as pure angular and pure stretching motions. The repulsive part of this NOCl excited potential energy surface is fit to *ab initio* calculations.

The different coordinate systems used for describing the ground and excited surfaces lead to three-dimensional nonseparable transition anplitudes, which are reduced to analytical forms by introduction of our infinite order sudden and Airy approximations for the continuum wave function and a quadrature formula for the integral over bending motions. Morse and co-workers[14] have previously presented approximate analytical IOS approximation computations of fragment rotational distributions as functions of initial rotational state (J,K), providing the first prediction for the mapping of the ground state bending vibration on the fragment rotational distributions. This earlier work, however, introduces several convenient approximations that are lifted here, including the retention of bend–stretch coupling and the use of anisotropic repulsive potentials for the continuum, as these features of the theory are important for an accurate description of dissociation processes.

The strong bend–stretch couplings present in the ν_2 and ν_3 modes of NOCl are again found to profoundly influence the predicted fragment rotational distributions. Calculated $K=0$, $J\neq 0$ diatomic photofragment rotational distributions are compared with a previous semiclassical approximation in order to illustrate the role of the mapping of the initial state bending wave function onto the fragment rotational distribu-

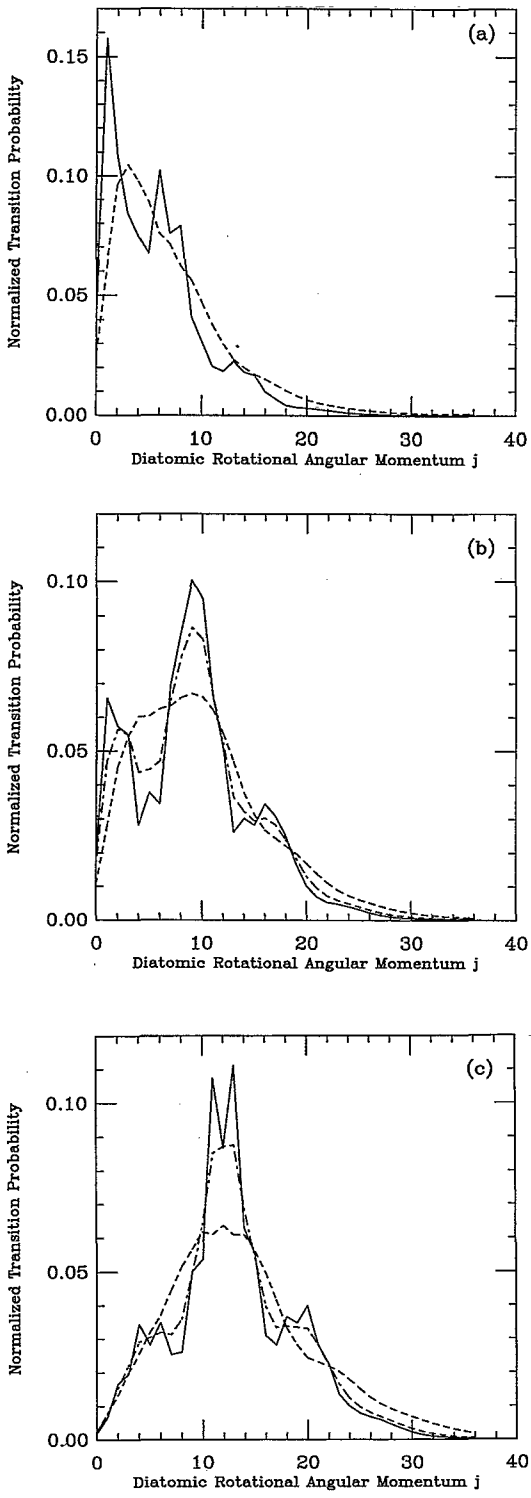

FIG. 5. Normalized thermally averaged IOS quantum-mechanical rotational fragment distributions for NOCl photodissociation under dipole coupling. (a) $n_1=n_2=n_4=0$; $n_3=0$. (—) $T=1$ K; (---) $T=3$ K. (b) $n_1=n_2=n_4=0$; $n_3=1$. (—) $T=1$ K; (·····) $T=2$ K; (---) $T=3$ K. (c) Same as (b), but $n_3=2$.

tions. Although this semiclassical approach reflects the nodal patterns of the initial bending wave function, our full IOS quantum-mechanical calculations have a more complex structure than the semiclassical counterpart, a behavior which emerges from the inclusion of the bend–stretch couplings in our analytical theory in addition to the use of an anisotropic potential energy surface and the incorporation of some slowly varying factors in the integral of Eq. (2.6). It should be emphasized that the present theory readily permits calculation of rotational distributions to be performed for any $J>0$ (and all K) without any additional computational effort, a technically difficult problem for close coupled theories because of the large number of channels which must be included for large J. In fact, the computation of thermally averaged rotational distributions for $T\leqslant 10$ K have required our computations for all $J,K\leqslant 9$. This has been done for nine initial vibrational states to illustrate the role of the mapping of the ground state bend and the coupling between pure angular and stretching motions.

The present computations are not compatible with the experiments on NOCl T_1 state photodissociation because the latter is observed to be an indirect process, whereas the present computations of a direct photodissociation therefore represent a model. (Work is in progress to deal analytically with indirect and nonadiabatic photodissociations.) The computations, however, indicate that the fast oscillations in the fragment rotational distributions for a single J,K initial state are transformed already for $T=3$ K into fairly broad fragment rotational distributions when a thermal average is performed over the initial rotational states.

ACKNOWLEDGMENTS

This research is supported by a National Science Foundation Grant (No. NSF CHE 9307489). We are grateful to L. Butler for her comments and critical reading of the manuscript. We would also like to thank M. D. Morse, H. Reisler, J. A. Beswick, and N. Halberstadt for helpful discussions. One of us (H.G.) wishes to thank to the Universidad de Buenos Aires and Consejo Nacional de Investigaciones Científicas y Técnicas (CONICET), República Argentina, for research grants and for a leave of absence to the James Franck Institute during parts of 1992–93 when this work was implemented. He also wishes to acknowledge to the James Franck Institute, University of Chicago, for providing the necessary relaxed and stimulating atmosphere.

[1] K. F. Freed and Y. B. Band, *Excited States*, edited by E. C. Lin (Academic, New York, 1977), Vol. 3, p. 109.
[2] J. A. Beswick and J. Jortner, Adv. Chem. Phys. **47**, 363 (1981).
[3] S. R. Leone, Adv. Chem. Phys. **50**, 255 (1982).
[4] (a) M. Shapiro and R. Bersohn, Annu. Rev. Phys. Chem. **33**, 409 (1982); (b) P. Brumer and M. Shapiro, Adv. Chem. Phys. **60**, 371 (1985).
[5] (a) R. Schinke, Annu. Rev. Phys. Chem. **39**, 39 (1988); (b) Comments At. Mol. Phys. **23**, 15 (1989); (c) in *Collision Theory for Atoms and Molecules*, edited by F. A. Gianturco (Plenum, New York, 1989), p. 229.
[6] (a) R. W. Heather and J. C. Light, J. Chem. Phys. **78**, 5513 (1983); (b) **79**, 147 (1983).
[7] Y. B. Band and K. F. Freed, Chem. Phys. Lett. **28**, 328 (1974).
[8] (a) Y. B. Band and K. F. Freed, J. Chem. Phys. **63**, 3382 (1975); (b) **63**, 4479 (1975); (c) **64**, 4329 (1976); (d) **67**, 1462 (1977).
[9] O. Atabek, J. A. Beswick, R. Lefebre, S. Mukamel, and J. Jortner, J. Chem. Phys. **65**, 4035 (1976).
[10] J. A. Beswick and W. M. Gelbart, J. Phys. Chem. **84**, 3148 (1980).
[11] M. Morse and K. F. Freed, Chem. Phys. Lett. **74**, 49 (1980).
[12] M. D. Morse and K. F. Freed, J. Chem. Phys. **74**, 4395 (1981).
[13] N. Halberstadt and J. A. Beswick, Faraday Discuss. Chem. Soc. **73**, 357 (1983).

[14] M. D. Morse and K. F. Freed, J. Chem. Phys. **78**, 6045 (1983).
[15] M. D. Morse, Y. B. Band, and K. F. Freed, J. Chem. Phys. **78**, 6066 (1983).
[16] O. Atabek, J. A. Beswick, and G. Delgado-Barrio, J. Chem. Phys. **83**, 2954 (1985).
[17] J. L. Krause, K. C. Kulander, and J. C. Light, J. Chem. Phys. **96**, 4283 (1992).
[18] H. Grinberg, K. F. Freed, and C. J. Williams, J. Chem. Phys. **86**, 5456 (1987).
[19] H. Grinberg, K. F. Freed, and C. J. Williams, J. Chem. Phys. **92**, 7283 (1990).
[20] H. Grinberg, K. F. Freed, and C. J. Williams, Chem. Phys. Lett. **182**, 297 (1991).
[21] (a) M. J. Berry, Chem. Phys. Lett. **27**, 73 (1974); (b) **29**, 329 (1974).
[22] Y. B. Band, M. D. Morse, and K. F. Freed, J. Chem. Phys. **68**, 2702 (1978).
[23] Y. B. Band, M. D. Morse, and K. F. Freed, Chem. Phys. Lett. **67**, 294 (1979).
[24] (a) M. D. Morse, K. F. Freed, and Y. B. Band, Chem. Phys. Lett. **44**, 125 (1976); (b) **49**, 399 (1977).
[25] (a) M. D. Morse, K. F. Freed, and Y. B. Band, J. Chem. Phys. **70**, 3604 (1979); (b) **70**, 3620 (1979).
[26] (a) C. X. W. Qian, A. Ogai, L. Iwata, and H. Reisler, J. Chem. Phys. **89**, 6547 (1988); (b) **92**, 4296 (1990).
[27] A. Ogai, C. X. W. Qian, and H. Reisler, J. Chem. Phys. **93**, 1107 (1990).
[28] (a) R. Schinke and V. Engel, J. Chem. Phys. **83**, 5068 (1985); (b) Faraday Discuss. Chem. Soc. **82**, 111 (1986).
[29] (a) R. Schinke, M. Nonella, H. U. Suter, and J. R. Huber, J. Chem. Phys. **93**, 1098 (1990).
[30] R. Schinke, J. Chem. Phys. **92**, 2397 (1990).
[31] R. Schinke, R. L. Vander Wal, J. L. Scott, and F. F. Crim, J. Chem. Phys. **94**, 283 (1991).
[32] A. Vegiri, A. Untch, and R. Schinke, J. Chem. Phys. **96**, 3688 (1992).
[33] D. J. Kouri, in *Atom–Molecule Collision Theory*, edited by R. B. Bernstein (Plenum, New York, 1979).
[34] Y. B. Band, K. F. Freed, and D. J. Kouri, J. Chem. Phys. **74**, 4380 (1981).
[35] E. Segev and M. Shapiro, J. Chem. Phys. **78**, 4969 (1983).
[36] Y. Y. Bai, A. Ogai, C. X. W. Qian, L. Iwata, G. A. Segal, and H. Reisler, J. Chem. Phys. **90**, 3903 (1989).
[37] M. E. Rose, *Elementary Theory of Angular Momentum* (Wiley, New York, 1957).
[38] R. N. Zare, *Angular Momentum* (Wiley, New York, 1988).
[39] C. C. Costain, in *Physical Chemistry—An Advanced Treatise*, edited by D. Henderson (Academic, New York, 1970), Vol. 4, p. 38.
[40] C. Cohen-Tannoudji, B. Diu, and F. Laloë, *Quantum Mechanics* (Wiley, New York, 1977), Vol. 1, p. 500.
[41] E. B. Wilson, J. C. Decius, and P. C. Cross, *Molecular Vibrations* (Dover, New York, 1955).
[42] D. M. Brink and G. R. Satchler, *Angular Momentum*, 2nd ed. (Clarendon, Oxford, 1975).
[43] *Handbook of Mathematical Functions*, edited by M. Abramowitz and I. A. Stegun (Dover, New York, 1970), p. 789.
[44] L. H. Jones, R. R. Ryan, and L. B. Asprey, J. Chem. Phys. **49**, 581 (1968).
[45] J. K. McDonald, J. A. Merrit, V. F. Kalasinsky, H. F. Heusel, and J. R. Durig, J. Mol. Spectrosc. **117**, 69 (1986).
[46] *JANAF Thermochemical Tables*, 2nd ed., edited by D. R. Stull and H. Prophet, Natl. Stand. Ref. Data Ser., Natl. Bur. Stand (U.S. GPO, Washington, DC, 1967).